Optimal Operation of a Membrane Reactor Network

Erik Esche
Chair of Process Dynamics and Operation, Berlin University of Technology, Sekr. KWT-9, Str. des 17. Juni 135, D-10623 Berlin, Germany

Harvey Arellano-Garcia
School of Engineering, Design and Technology, University of Bradford, West Yorkshire BD7 1DP, U.K

Lorenz T. Biegler
Dept. of Chemical Engineering, Carnegie Mellon University, 5000 Forbes Avenue, Pittsburgh, PA 15213

DOI 10.1002/aic.14252
Published online October 25, 2013 in Wiley Online Library (wileyonlinelibrary.com)

In this contribution, the operation of a membrane reactor network (MRN) for the oxidative coupling of methane is optimized. Therefore, three reactors, a fixed bed reactor (FBR) and two packed bed-membrane reactors, are modeled. For the (CPBMR), a two-dimensional (2-D) model is presented. This model incorporates radial diffusion and thermal conduction. In addition, two 10 cm long cooling segments for the CPBMR are implemented based on the idea of a fixed cooling temperature positioned outside the reactor shell. The model is discretized using a newly developed 2-D orthogonal collocation on finite elements with a combination of Hermite for the radial and Lagrangian polynomials for the axial coordinate. Membrane thickness, feed compositions, temperatures at the inlet and for the cooling, diameters, and the amount of inert packing in the reactors are considered as decision variables. The optimization results in C_2 yields of up to 40% with a selectivity in C_2 products of more than 60%. The MRN consisting of an additional packed-bed membrane reactor with an alternative feeding policy and a FBR shows a lower yield than the individual CPBMR.
 AIChE J, 60: 170–180, 2014
Keywords: OCM, membrane reactor network, orthogonal collocation, large-scale NLP

Motivation and Introduction

For remote, isolated wells of natural gas, a combination of steam reforming and Fischer-Tropsch synthesis is often applied to turn methane into more easily transportable and chemically processable hydrocarbons. However, this process demands enormous amounts of energy as noted by Unruh et al.[1] and has an efficiency between 25 and 50% depending on reactant compositions and operating conditions. An alternative to this process is the oxidative coupling of methane (OCM), which according to Jašo et al.[2] has the potential to become a key technology in the chemical industry. The OCM process allows for direct production of alkenes (olefins) or alkanes from methane (CH_4). It skips the energy intensive syngas formation (steam reforming) and could thus potentially be more energetically and economically efficient. Hence, this process offers various opportunities for replacing oil with natural gas.

As part of the cluster of excellence "Unifying Concepts in Catalysis" (UniCat)*, a mini-plant is being built at the Berlin University of Technology (Technische Universität Berlin) to investigate the technical viability of the OCM process on a larger scale. This contribution deals with the modeling and optimization of a part of that mini-plant, namely, a membrane reactor network (MRN).

OCM has many challenges such as its exothermic nature and the undesired simultaneous creation of carbon oxides. Therefore, any practical application should allow for adequate temperature control and low oxygen levels. To investigate these effects several apparatuses as well as various catalysts have already been tested: In a fixed-bed reactor (FBR) particles or pellets in the bed carry the required catalyst. In a classical FBR, the equilibrium composition can ideally be attained at the outlet and the product streams need to be further processed to extract ethylene and other hydrocarbons. The same is true for a fluidized bed reactor which allows for almost isothermal reactor conditions, but requires a catalyst with a high-mechanical stability. A more promising approach has been developed by Lafarga et al.[3] in the form of packed-bed membrane reactors (PBMRs), which offer additional benefits by gradually feeding oxygen to the catalyst so as to allow for a higher selectivity in C_2 products, meaning lower carbon oxide formation. PBMRs are comparatively simple in their process design and safer in operation than an FBR (see Quddus et al. [4] for details). They not only provide enhanced catalytic activity and selectivity, but also include the product separation.

Despite these advantages, a permeable membrane also implies loss of reactants by diffusion to the noncatalytic side of the reactor. One measure, which reduces this effect, is the introduction of a recycle stream feeding a part of a product

Correspondence concerning this article should be addressed to E. Esche at erik.esche@tu-berlin.de.
*For further information on UniCat visit http://www.unicat.tu-berlin.de.

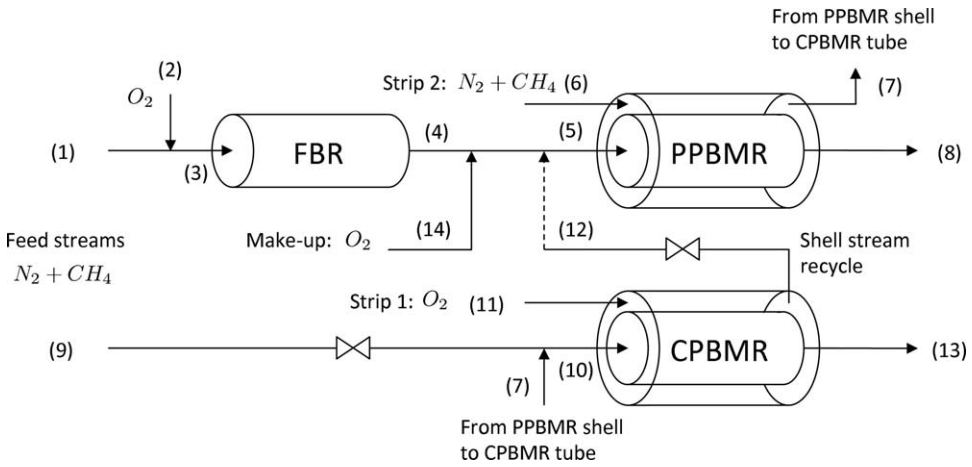

Figure 1. Flowsheet of the proposed MRN.

Figure redrawn in accordance with Godini et al.[6]

stream back into the system, which Chan[5] discusses in detail. Following this concept, Figure 1 shows the MRN proposed by Godini et al.[6] The network consists of three reactors: a common FBR and two PBMRs, which only differ in their feeding policy (CPBMR and PPBMR).

Given the strongly different performance of all three reactors in the system, building and operating the network without previous modeling and simulation will be difficult. In addition, the number of possible decision variables for the system, that is catalysts, length of reactors, feed concentrations, and temperatures and so forth, is so high that a simple sensitivity analysis based on simulations will not suffice. For this reason, this contribution optimizes the operation of the network shown earlier by manipulating both geometrical and operational parameters to maximize the overall yield. Necessary to that end is the derivation of suitable reactor models, the development of a stable discretization method, and the application of a suitable optimization algorithm.

The following chapters present a brief overview on how all three reactors are modeled and discretized before discussing the simulation and optimization of the MRN.

Status Quo

PBMRs have already been simulated quite extensively. However, most simulations only considered one-dimensional (1-D) models. For some applications comparable to the OCM, such as the dehydrogenation of butane (Téllez et al.[7]) a neat agreement between experiments and 1-D models was observed for most species appearing in the kinetics. Similarly, Diakov and Varma[8] were able to use an experimentally validated, 1-D model to optimize the feed distribution in a membrane reactor for the dehydrogenation of methanol. Other successfully implemented simulations included the steam reforming of methane (Barbieri and Maio[9]) and the decomposition of H_2S (Chan et al.[10]), both carried out 1-D.

Despite all this, there seem to be cases in which a more rigorous model is required, even for reactors with smaller diameters. Al-Juaied et al.[11] investigated the epoxidation of ethylene in a catalytic PBMR using 1-D models. They concluded among other things that a proper description of the diffusive flux through the membrane is rather important. In previously conducted work by Jašo et al.,[2,12] only 1-D models for the three aforementioned reactors were applied to investigate the attainable performance. Their investigations included the influence of operating temperature, membrane thickness, methane-to-oxygen ratio, overall feed flow rates, gas stream compositions, and reactor lengths. They observed very strong discrepancies, that is, overestimations, to any experimentally found reactor yields.

To this end, Tóta et al.[13] present a conclusive overview of PBMRs and their simulation in general. They consider 1-D, 2-D as well as three-dimensional models incorporating everything from radial dispersion to local velocity profiles. As a case study, they focus on the dehydrogenation of ethane to ethylene, which is a reaction step that reappears in the OCM. They highlight the importance of proper rigorous modeling, pointing out that their 1-D models led to an overestimation of the reactor performance compared to the two-dimensional (2-D) version.

Model Derivation

The kinetics of the La_2O_3/CaO catalyst considered for this contribution and derived by Stansch et al.[14] are known to be quite fast. This could imply that the oxygen permeating from the shell-side of the CPBMR through the membrane into the tube-side reacts fairly quickly after entering the catalytic bed. This could cause the appearance of steep radial concentration and temperature gradients. For this reason, a 2-D model is envisioned for the CPBMR. However, because of the intended optimization and, therefore, required lower computational complexity, only radial diffusion and heat conduction will be included initially. The same effect should not appear or not appear as strongly in the other two reactors, which remain 1-D for now. This chapter introduces all major assumptions, the reaction kinetics, as well as the individual reactor models.

General assumptions

All gases are assumed to behave as perfect or ideal gases. Correlations published by Kleiber and Joh[15] are used to calculate viscosities, thermal conductivities of pure components and so forth.

Fuller et al.[16] present a semitheoretical, semiempirical function for the calculation of binary diffusion coefficients. Using these, Kee et al.[17, p. 528] introduced mixture averaged diffusion coefficients, which are applied for the reactor's shell-sides here. The packed-beds impede the radial diffusion and the axial flow of gases. In this contribution, an approach

suggested by Tsotsas and Schlünder[18] is used that has already been successfully applied to a PBMR. A radial effective dispersion coefficient is defined for each component as the sum of a molecular and a crossmixing term, wherein the molecular term may be calculated in accordance with Kee et al.'s correlation.[13, p. 117]

The flux of any component through the membranes is calculated with the help of Kundsen's diffusivity theory as has been experimentally shown by Lafarga et al.[3, p. 2011] The membrane thickness is varied around 50 μm, the pore radius is 2 nm, the membrane porosity lies at 0.5, and the tortuosity at 2.95. Hence, the investigated application falls into the region discussed by Lafarga et al. The flux through the membrane is a function of the concentrations on either side of the membrane and Knudsen's diffusion coefficients. These in turn are inversely proportional to the square root of the molar mass of each component. Diffusion is assumed to be the only radial transport mechanism. Therefore, the flux through the membrane of a component i on either side can also be described with Fick's law.

For the thermal conductivity of the gas mixtures, a model presented by Kleiber and Joh[15, p. Da 26] may be used. To combine individual thermal conductivities into a single one for the whole mixture, the rule developed by Wassiljeva et al.[19] is applied. Several approaches exist, which describe the effective radial thermal conductivity λ_{eff} in a packed-bed. A model for the radial thermal conduction published by Bauer and Schlünder[20,21] is used.

The diffusive mass transport through the membranes brings about an enthalpy flow $\dot{h}_{\text{membrane}}$ and conduction of the membranes themselves enables a heat transfer $\dot{q}_{\text{membrane}}$ between both sides:

$$\dot{q}_{\text{membrane}} = k_{\text{membrane}} \cdot \left(T_{\text{tube}}\left(r=r_{\text{tube}}, z\right) - T_{\text{shell}}\left(r=r_{\text{tube}}, z\right)\right) \tag{1}$$

$$\dot{h}_{\text{membrane}} = \sum_{i=1}^{NC} \left(\dot{n}_{i,\text{diff}} \cdot c_{p,i}\right) \cdot \left(T_{\text{tube}}\left(r=r_{\text{tube}}, z\right) - T_{\text{shell}}\left(r=r_{\text{tube}}, z\right)\right) \tag{2}$$

Specchia et al.[22] published correlations for the calculation of heat transfer coefficients of walls adjoining catalytic packed-beds. For 1-D cases, a correlation has been developed by Dixon.[23]

Reaction kinetics

As mentioned, the kinetic model of Stansch et al.[14] is used in this contribution. Their reaction mechanism is based on the following ten reactions:

$$CH_4 + 2\cdot O_2 \rightarrow CO_2 + 2\cdot H_2O \tag{R1}$$

$$2\cdot CH_4 + \frac{1}{2}\cdot O_2 \rightarrow C_2H_6 + H_2O \tag{R2}$$

$$CH_4 + O_2 \rightarrow CO + H_2O + H_2 \tag{R3}$$

$$CO + \frac{1}{2}\cdot O_2 \rightarrow CO_2 \tag{R4}$$

$$C_2H_6 + \frac{1}{2}\cdot O_2 \rightarrow C_2H_4 + H_2O \tag{R5}$$

$$C_2H_4 + 2\cdot O_2 \rightarrow 2\cdot CO + 2\cdot H_2O \tag{R6}$$

$$C_2H_6 \rightarrow C_2H_4 + H_2 \tag{R7}$$

$$C_2H_4 + 2\cdot H_2O \rightarrow 2\cdot CO + 4\cdot H_2 \tag{R8}$$

$$CO + H_2O \rightarrow CO_2 + H_2 \tag{R9}$$

$$CO_2 + H_2 \rightarrow CO + H_2O \tag{R10}$$

Only reaction R7 therein takes place in the gas phase, all others are surface reactions. Additionally, reactions R1 to R6 are inhibited by carbon dioxide adsorbed on the catalytic surface, which is also shown by the kinetics. The component rate $\dot{c}r_i$ for component $i, \forall i \in \{1, \ldots, 9\}$, can be calculated according to Eq. 3. The ninth component herein is nitrogen, which is considered to be inert.

$$\dot{c}r_i = \varphi_{\text{cat}} \cdot \rho_{\text{cat}} \cdot \sum_{j=\text{R1}}^{\text{R6}} A_{i,j} \cdot \dot{rr}_j + (1-\varphi_{\text{cat}}) \cdot A_{i,\text{R7}} \cdot \dot{rr}_{\text{R7}} + \varphi_{\text{cat}} \cdot \rho_{\text{cat}} \cdot \sum_{j=\text{R8}}^{\text{R10}} A_{i,j} \cdot \dot{rr}_j \tag{3}$$

A is a matrix of stoichiometric coefficients for all components in the reactions above, and $\dot{r}r_j$ is the rate of reaction j. Equations 4–9 present details on how the reaction rates $\dot{r}r_j$ for all 10 reactions are calculated.

$$\dot{r}r_j = \frac{k_{0,j} \cdot e^{\frac{-E_{A,j}}{\bar{R}}\cdot T} \cdot p_C^{m_j} \cdot p_{O_2}^{n_j}}{\left(1 + K_{j,CO_2} \cdot e^{\frac{-\Delta H_{ad,CO_2,j}}{\bar{R}}\cdot T} \cdot p_{CO_2}\right)^2}, \quad \forall j \in \{\text{R1}, \text{R3}, \ldots, \text{R6}\} \tag{4}$$

$$\dot{r}r_{\text{R2}} = \frac{k_{0,\text{R2}} \cdot e^{\frac{-E_{A,\text{R2}}}{\bar{R}\cdot T}} \cdot \left(K_{O_2} \cdot e^{\frac{-\Delta H_{ad,O_2}}{\bar{R}}\cdot T} \cdot p_{O_2}\right)^{n_{\text{R2}}} \cdot p_{CH_4}^{m_{\text{R2}}}}{\left(1 + \left(K_{O_2} \cdot e^{\frac{-\Delta H_{ad,O_2}}{\bar{R}}\cdot T} \cdot p_{O_2}\right)^{n_{\text{R2}}} + K_{\text{R2},CO_2} \cdot e^{\frac{-\Delta H_{ad,CO_2,\text{R2}}}{\bar{R}}\cdot T} \cdot p_{CO_2}\right)^2} \tag{5}$$

$$\dot{r}r_{\text{R7}} = k_{0,\text{R7}} \cdot e^{\frac{-E_{A,\text{R7}}}{\bar{R}}\cdot T} \cdot p_{C_2H_6} \tag{6}$$

$$\dot{r}r_{\text{R8}} = k_{0,\text{R8}} \cdot e^{\frac{-E_{A,\text{R8}}}{\bar{R}}\cdot T} \cdot p_{C_2H_4}^{m_{\text{R8}}} \cdot p_{H_2O}^{n_{\text{R8}}} \tag{7}$$

$$\dot{r}r_{\text{R9}} = k_{0,\text{R9}} \cdot e^{\frac{-E_{A,\text{R9}}}{\bar{R}}\cdot T} \cdot p_{CO}^{m_{\text{R9}}} \cdot p_{H_2O}^{n_{\text{R9}}} \tag{8}$$

$$\dot{r}r_{\text{R10}} = k_{0,\text{R10}} \cdot e^{\frac{-E_{A,\text{R10}}}{\bar{R}}\cdot T} \cdot p_{CO_2}^{m_{\text{R10}}} \cdot p_{H_2}^{n_{\text{R10}}} \tag{9}$$

p_C in Eq. 4 represents the partial pressure of the reagent in the respective reaction containing carbon. Values for the coefficients $k_{0,j}, E_{A,j}$ etc. appearing in Eqs. 4 to 9 have been published by Stansch et al.[14]

The FBR model

The 1-D model for the FBR consists of the following differential equations describing concentration and temperature profiles

$$\frac{\partial c_i}{\partial z} = \frac{\dot{c}r_i}{u_z} \tag{10}$$

$$\frac{\partial T}{\partial z} = \frac{-k_{OS} \cdot (T(z) - T_{\text{cool}}) \cdot 2 + \sum_{j=1}^{NR} \left(\varphi_{\text{cat}} \cdot \varrho_{\text{cat}} \cdot \dot{rr}_j \cdot (-\Delta_R H)\right) \cdot r_{\text{FBR}}}{c_{\text{tot}} \cdot c_{p,\text{mix}} \cdot u_z \cdot r_{\text{FBR}}} \tag{11}$$

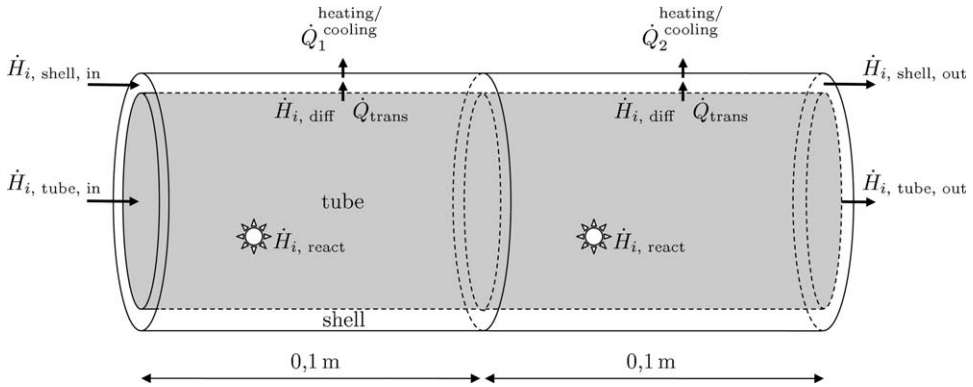

Figure 2. Sketch for the heated or cooled model of the CPBMR.

The reactor is heated or cooled through its lateral, outer shell. T_{cool} is the temperature of the cooling jacket and k_{OS} the respective heat transfer coefficient.

The PPBMR model

For the PPBMR the influence of the membrane and the shell-side of the reactor need to be added to the set of differential equations. Consequently, each side has its own equations for concentrations and temperatures as follows

$$u_{z,T}\cdot\pi\cdot r_{\text{tube}}^2\frac{\partial c_{i,\text{tube}}}{\partial z}\cdot dz = \dot{cr}_i\cdot\pi\cdot r_{\text{tube}}^2\cdot dz - d\dot{N}_{i,\text{diff}}(z) \quad (12)$$

$$u_{z,S}\cdot\pi\cdot\left(r_{\text{shell}}^2-r_{\text{tube}}^2\right)\cdot\frac{\partial c_{i,\text{shell}}}{\partial z}\cdot dz = d\dot{N}_{i,\text{diff}}(z) \quad (13)$$

$$\frac{\partial T^T}{\partial z} = \frac{\sum_{j=1}^{NR}\left(\varphi_{\text{cat}}\cdot\tilde{n}_{\text{cat}}\cdot\dot{rr}_j\cdot(-\Delta_R H)\right)\cdot\pi\cdot r_T^2}{c_{\text{tot}}^T\cdot c_{p,\text{mix}}^T\cdot u_z^T\cdot\pi\cdot r_T^2} - \frac{\dot{h}_{\text{diff}}\cdot 2\cdot\pi\cdot r_S}{c_{\text{tot}}^T\cdot c_{p,\text{mix}}^T\cdot u_z^T\cdot\pi\cdot r_T^2} - \frac{\dot{q}_{\text{trans}}\cdot 2\cdot\pi\cdot r_S}{c_{\text{tot}}^T\cdot c_{p,\text{mix}}^T\cdot u_z^T\cdot\pi\cdot r_T^2} \quad (14)$$

$$\frac{\partial T^S}{\partial z} = \frac{\dot{h}_{\text{diff}}\cdot 2\cdot\pi\cdot r_S}{c_{\text{tot}}^S\cdot c_{p,\text{mix}}^S\cdot u_z^S\cdot\pi\cdot\left(r_S^2-r_T^2\right)} + \frac{\dot{q}_{\text{trans}}\cdot 2\cdot\pi\cdot r_S}{c_{\text{tot}}^S\cdot c_{p,\text{mix}}^S\cdot u_z^S\cdot\pi\cdot\left(r_S^2-r_T^2\right)} - \frac{k_{OS}\cdot(T^S(z)-T_{\text{cool}})\cdot 2\cdot\pi\cdot r_S}{c_{\text{tot}}^S\cdot c_{p,\text{mix}}^S\cdot u_z^S\cdot\pi\cdot\left(r_S^2-r_T^2\right)} \quad (15)$$

The CPBMR model

Figures 3a, b show a sketch of the CPBMR and a differential volume element of its tube-side, respectively. Hence, the mass balance for the tube-side leads to

$$0 = -u_z\cdot\frac{\partial c_i(r,z)}{\partial z} + \mathrm{D}_{i,r}\cdot\left[\frac{\partial^2 c_i}{\partial r^2}+\frac{1}{r}\cdot\frac{\partial c_i}{\partial r}\right] + \dot{cr}_i \quad (16)$$

and for the shell-side respectively

$$0 = -u_z\cdot\frac{\partial c_i(r,z)}{\partial z} + \mathrm{D}_{i,r}\cdot\left[\frac{\partial^2 c_i}{\partial r^2}+\frac{1}{r}\cdot\frac{\partial c_i}{\partial r}\right]. \quad (17)$$

The 2-D modeling moves the equations for the heat transfer through the outer shell and the membrane to the boundary conditions. A differential energy balance of the tube-side of the CPBMR leads to

$$c_{\text{tot}}\cdot c_{p,\text{tot}}\cdot u_z\cdot\frac{\partial T}{\partial z} = \lambda\cdot\left[\frac{\partial^2 T}{\partial r^2}+\frac{1}{r}\cdot\frac{\partial T}{\partial r}\right] + \sum_{j=1}^{NR}\left(\varphi_{\text{cat}}\cdot\tilde{n}_{\text{cat}}\cdot\dot{rr}_j\cdot(-\Delta_R H)\right). \quad (18)$$

For the description of the shell-side, the reaction term is simply left out

$$c_{\text{tot}}\cdot c_{p,\text{tot}}\cdot u_z\cdot\frac{\partial T}{\partial z} = \lambda\cdot\left[\frac{\partial^2 T}{\partial r^2}+\frac{1}{r}\cdot\frac{\partial T}{\partial r}\right]. \quad (19)$$

Figure 2 shows the basic idea of the heated or cooled model for the CPBMR. Each 10-cm segment of the reactor can be cooled or heated separately through the outer shell according to

$$\dot{q}_{\text{heat/cool}}(z) = k_{\text{OS}}\cdot\left(T(r=r_{\text{shell}},z)|_{\text{shell}}-T_{\text{cool}}\right) \quad (20)$$

$$= -\lambda_{\text{mix}}^G(r=r_{\text{shell}},z)\cdot\frac{\partial T}{\partial r}|_{\text{shell}}. \quad (21)$$

Further introduction of axial dispersion and local velocity fields as suggested by Tóta et al.[13] is not planned at this point in order to keep the size of the problem at a reasonable level for optimization. Given that the Reynolds number of the packed bed (~30) is somewhere in the transitional region, closer to the laminar side, the effects of the axial dispersion can possibly be neglected.

Collocation

As the MRN is supposed to be optimized using a simultaneous optimization approach, a highly stable discretization method is required for handling the partial differential equations (PDE*s*) shown earlier. Therefore, all differential equations in this contribution are discretized by applying orthogonal collocation on finite elements. Third-order Lagrangian polynomials are used to collocate any ordinary differential equations using Radau roots to guarantee the continuity of each variable across finite elements as described by Biegler.[24, p.288ff] For PDEs a combination of Hermite and Lagrangian polynomials is derived.

Collocation derivation

In case, second-order derivatives appear in a differential equation, the continuity of first-order derivatives across finite elements needs to be ensured. For this application, Hermite cubic polynomials are of advantage. Their usage guarantees the continuity of the function itself and its first derivative

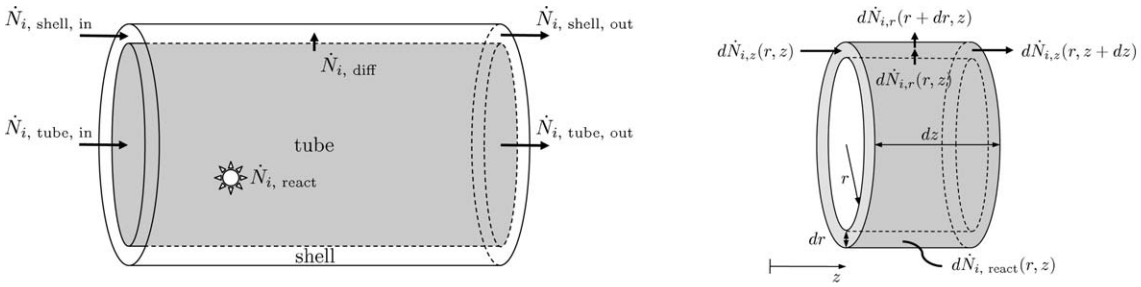

(a) Sketch of the *CPBMR* for the isothermal model.

(b) Differential segment of the tube-side of the *CPBMR* for the isothermal model.

Figure 3. Balance volume for the derivation of the isothermal model for the CPBMR.

between two adjoining finite elements. The polynomials used forthwith are taken from Finlayson,[25, p. 272] who used Hermite polynomials for the 2-D discretization of a sphere.

The basic idea of extending the 1-D orthogonal collocation to a second dimension is to use different functions for each direction, which depend on different variables and then to multiply both of them

$$c_{LH}(u,v)=\left(\sum_{l=1}^{4} a_{u,l}\cdot \ell_l(u)\right)\cdot\left(\sum_{l=1}^{4} a_{v,l}\cdot \mathrm{H}_l(v)\right). \tag{22}$$

Equation 22 can also be written as follows wherein $a_{i,j}=a_{u,i}\cdot a_{v,j}$:

$$c_{LH}(u,v)=a_{1,1}\cdot\ell_1(u)\cdot \mathrm{H}_1(v)+a_{1,2}\cdot\ell_1(u)\cdot \mathrm{H}_2(v)+a_{1,3}\cdot\ell_1(u)\cdot\mathcal{H}_3(v) \tag{23}$$

$$+a_{1,4}\cdot\ell_1(u)\cdot \mathrm{H}_4(v)+a_{2,1}\cdot\ell_2(u)\cdot \mathrm{H}_1(v)+\ldots+a_{4,4}\cdot\ell_4(u)\cdot \mathrm{H}_4(v) \tag{24}$$

The new approximation function, which is basically a surface function, contains 16 coefficients $a_{i,j}$, half of which assume the value of the collocated variable at certain collocation positions $(a_{0,1}, a_{1,1}, \ldots, a_{0,3}, a_{1,3}, \ldots)$ and the other half are the respective first, radial derivative $(a_{0,2}, a_{1,2}, \ldots, a_{0,4}, a_{1,4}, \ldots)$. This is depicted in Figure 4. To extend the approximating function c_{LH} to a second finite element or segment the respective collocation variables need to be forwarded (which would imply new equations) or reused (without additional equations) in the adjoining segment. One segment inherits four collocation variables from its axial predecessor and six from its radial predecessor.

Implementation

Application of the derived collocation methods for discretizing all reactor models leads to a large-scale non-linear programming (NLP), which is both highly nonlinear and nonconvex. The model for the CPBMR consists of roughly 130,000 equality constraints, about 5% of which are formulated as solely linear equations. In addition, 40,000 inequalities further constrain the system. In this case, twelve axial and five radial finite segments are defined, so a total of 60 finite segments. When using 1-D models for the additional reactors, the problem grows by roughly 30,000 equality constraints. The implementation leads to relative errors of mass and atom balances of below 10^{-5}.

In order to solve the NLP problem, it is coded in AMPL (see Fourer et al.[26] for details) and the interior point barrier method implemented in IPOPT (see Biegler et al.[24, p. 151 ff., 27] for details) is used. Tuning IPOPT (solver name) led to some measurable reductions of the convergence time of the whole system. By choosing MA57 from the Harwell Subroutine Library[28] as a linear solver and the Metis package for matrix reordering,[29] the convergence time could be reduced to less than 25% in comparison to the default configuration.

Given the form of the discretization method chosen for both the 1-D and 2-D models, a rather complicated initialization is required for setting up the optimization. The same procedure is also used for simply simulating the reactor: Initially, only the first axial segment is activated and set to a very short length. This segment can be resolved for a steadily increasing axial length. Once the required length is achieved, the first segment is frozen and the results are taken as starting points for the second axial segment which is initialized, again with a very short axial length. This method was found to be highly reliable to simulate the individual reactor and eventually also the whole network including all recycle streams. AMPL's scripting language has some very neat properties for fixing and unfixing variables and dropping bounds to properly implement this initialization.

Stand-Alone Operation of the CPBMR

Before simulating and optimizing the network, the more complex model of the CPBMR is investigated in more detail.

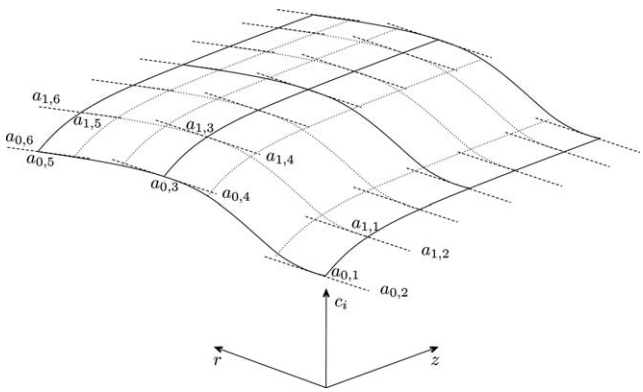

Figure 4. Depiction of the collocating surface function using Hermite and Lagrangian polynomials and the meaning of respective collocation variables.

Table 1. Operational and Geometrical Parameters of the CPBMR that may be Modified Within the Given Bounds

Parameter	Symbol	Value	Lower bound	Upper bound	Unit
Geometrical Parameters					
Diameter of tube	d_{tube}	0.007	0	d_{shell}	m
Diameter of shell	d_{shell}	0.010	d_{tube}	–	m
Membrane thickness	δ_{mem}	50	0.1	100	μm
Catalyst density	ϱ_{cat}	3600	0	3700	kg/m3
Catalyst volume fraction	φ_{cat}	0.64	0	1	–
Operational Parameters					
Temperature at inlet, shell-side	T^S_{Inlet}	1023.15	290	1375	K
Temperature at inlet, tube-side	T^T_{Inlet}	1023.15	290	1375	K
Cooling/heating temperature, seg. I	$T^I_{h/c}$	1023.15	290	1375	K
Cooling/heating temperature, seg. II	$T^{II}_{h/c}$	1023.15	290	1375	K
Molar fraction of oxygen, shell-side	$x^S_{O_2}$	0.128	0	1	–
Molar fraction of nitrogen, tube-side	$x^T_{CH_4}$	0.170	0	1	–

Simulation of the CPBMR

Preceding the optimization, extensive simulation studies are carried out. By making each of the aforementioned model parameters in turn dependent on local concentrations and temperatures, it could be found that all fluid properties and transport coefficients should in fact not be calculated with averaged concentrations and temperatures, but using locally dependent values instead. Neglecting the heat of reaction or the influence of the heat loss through the outer shell can have a big impact on the performance. Nonisothermal models should be preferred at all times.

A comparison between the 2-D and a 1-D model shows an overestimation of the reactor performance of the latter model in terms of yield in C_2 hydrocarbons by as many as 25% points.

Given the nonlinearity and scale of the model, a number of measures is tested to improve the convergence behavior such as avoiding nondifferentiable points, scaling of variables (e.g., using natural logarithms), linearizing constraints, and increasing the sparsity of matrices. These measures did not yield any considerable improvements. The main issue appears to be the bad scaling of the second-order derivatives, which cannot be resolved.

Optimization of the CPBMR

Table 1 contains a comprehensive list of operational and geometrical parameters of the CPBMR that may be modified within given bounds. For matters of problem size, additional possible decision variables are disregarded. Among those are the inlet pressures for shell- and tube-side, superficial velocities, and selection of the right type of catalyst. Similarly, the reactor length will be held constant at 20 cm, because of the difficulties related to removing or adding an entire heating/cooling segment, each of which is 10 cm long. The lower and upper bounds noted in Table 1 state what should be possible theoretically.

Table 2 shows the configuration and the performance at the starting point (0), an intermediate step (1), and the final optimization results (2). $_L$ and ^{U} assign active lower or upper bounds on decision variables, which are specified by the user. The reactor is assessed using Godini et al.'s[6] definitions of yield Y, selectivity S in C_2 hydrocarbons, and CH_4 conversion X.

Figure 5 shows the concentration profiles for ethylene and ethane and the temperature profile for the final optimization step noted in Table 2. The single optimization runs took between 20 min to several days depending on the initialization. The calculations were carried out on an AMD Opteron Processor 250 with 2.3 GHz and 16 GB of RAM.

Selectivity Target Analysis. While having a high yield in C_2 products is advantageous, the product gas still needs to be cleaned of both reactants and side-products, like carbon oxides, before further processing. The selectivity in C_2 hydrocarbons is a measure for how many of the reacted methane molecules formed hydrocarbons and how many carbon atoms went into the formation of carbon oxides: the lower the selectivity, the more carbon oxides are produced. The selectivities presented in the optimization results for the stand-alone operation of the CPBMR are already quite high ($\geq$ 60%). Nevertheless, it is examined to what extent it is possible to further increase the selectivity for a given optimal solution by enforcing a lower bound on the selectivity.

As a starting point, the intermediate step 1 in Table 2 is chosen. The yield in C_2 hydrocarbons at that point lies at roughly 44% while the selectivity is just above 68.5%. Apparently, an increase in the selectivity target of 1% point does not cause the yield to drop by less than that amount.

Table 2. Collection of Decision Variables for Three Steps in the Optimization of the CPBMR and Respective Performance

No.	T^S_{in} (K)	T^T_{in} (K)	$T^I_{h/c}$ (K)	$T^{II}_{h/c}$ (K)	$x^S_{O_2}$ (–)	$x^T_{CH_4}$ (–)
0	1023	1023	1023	1023	0.128	0.170
1	990_L	990_L	990_L	990_L	0.149^U	0.162_L
2	970_L	1013	970_L	970_L	0.157^U	0.128

No.	d_T (mm)	d_S (mm)	ϱ_{cat} (kg/m^3)	φ_{cat} (–)	δ_{mem} (μm)
0	7.0	10	3600	0.64	50
1	6.0_L	7.8_L	3700^U	0.70^U	62.4
2	6.0_L	7.8_L	3700^U	0.70^U	65^U

No.	Yield in C_2	Selectivity in C_2	Conversion of CH_4
0	0.303	0.550	0.551
1	0.441	0.686	0.643
2	0.469	0.633	0.740

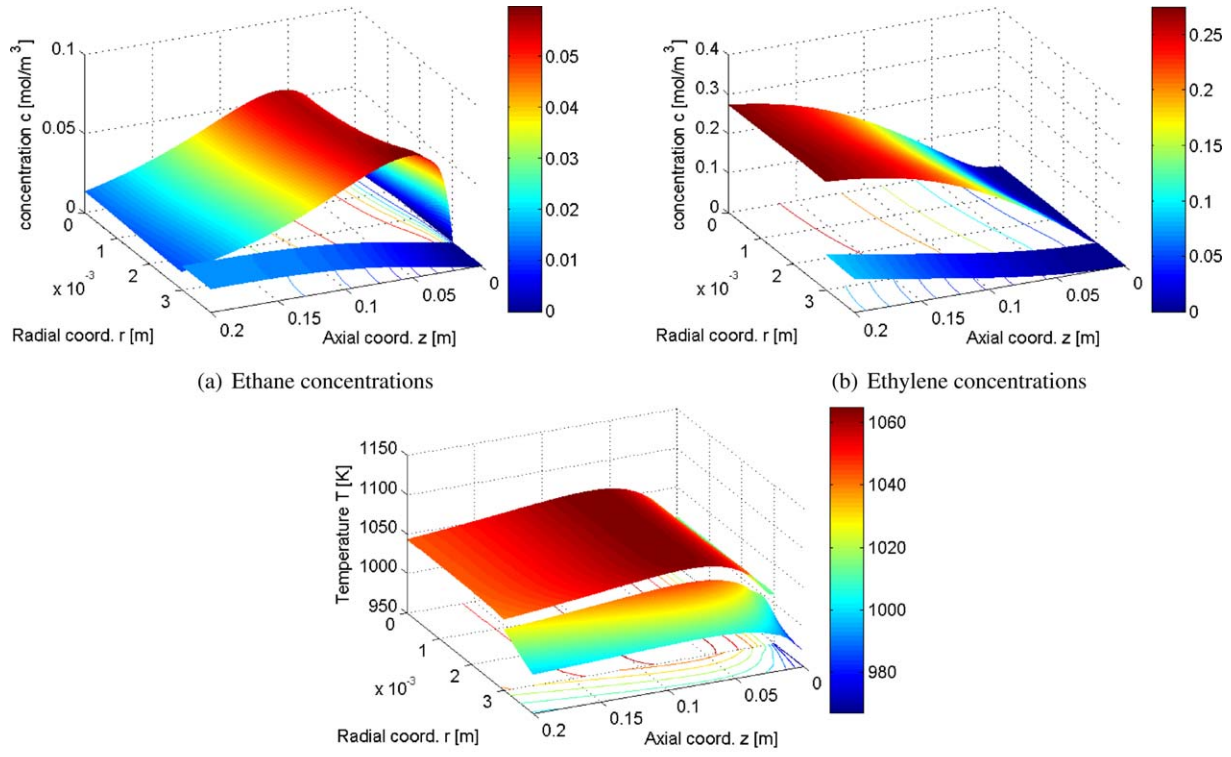

(a) Ethane concentrations

(b) Ethylene concentrations

(c) Temperature profile

Figure 5. Ethane, ethylene and temperature profiles for the last step of the CPBMR stand-alone optimization.

[Color figure can be viewed in the online issue, which is available at wileyonlinelibrary.com.]

Yield decreases seem to be getting slowly larger when surpassing a selectivity of 75%. Only 7 of the 11 decision variables stay at their original value comparing the starting point to the last step of the selectivity target optimization. The most obvious movement here is a shift to even higher methane to oxygen ratios in the packed-bed as both methane fraction and membrane thickness go up while the oxygen fraction goes down.

Discussion of results

Before proceeding to the next step–the integration of the CPBMR into the MRN–a short discussion of all results so far is in order.

The performance of the CPBMR reported herein is–with respect to the yield in C_2 hydrocarbons–better than expected and reaches higher levels than have ever experimentally been found.

In order to simulate and optimize the CPBMR successfully, five radial and twelve axial finite elements are required. However, this system seems to be touching its boundaries in the last few optimization studies carried out here. It is possible that with an even larger number of radial finite elements an even better performance with respect to the yield in C_2 hydrocarbons could be reached.

The incorporation of radial effects into the CPBMR model makes a difference and is vital for obtaining more sensible results in comparison to the 1-D case. It is exactly this radial influence that makes the simulation and optimization of the CPBMR complicated as it is mainly responsible for increasing the number of required variables by a factor of ten.

Overall, the general optimization of the CPBMR has confirmed some of the trends already found in a rough sensitivity analysis that was carried out on the decision variables:

1. There seems to be a general trend toward a thicker membrane. This obviously reduces the heat transfer between shell and tube, but the predominant effect seems to be the reduction of the molar flux of heavier molecules. Oxygen enters the tube through the membrane in the largest quantities, because of the large concentration difference between shell-side and tube-side. Consequently, the thicker the membrane the lower the oxygen flux, and thus, the lower the resulting oxygen concentrations in the reactor tube-side, which apparently ensure the highest possible yields. The oxygen levels found in simulations and optimizations of the CPBMR described earlier range between roughly zero and 500 Pa. What is interesting to see in this context is that there is–even at the outlet of the 20 cm long CPBMR–still a positive C_2 hydrocarbon formation rate. Common perception was that at that point the potential of methane conversion should be exhausted.
2. Inlet temperatures of both shell- and tube-side have dropped below the original 1023.15 K and the cooling jacket is extracting some 28.5 W from the reactor in addition to the heat transported away by the shell-side stream while ensuring an almost isothermal temperature level in the tube-side of the CPBMR, and thus, allowing for optimal operating conditions along the entire reactor length as shown in Figure 5c.
3. With respect to the catalytic bed, there seems to be a trend pointing at the minimization of the actual gas phase and covering as much of the packing with catalyst. However, this trend should not be overrated. A sensitivity analysis shows that the actual increase in the yield caused by this trend is comparatively small.

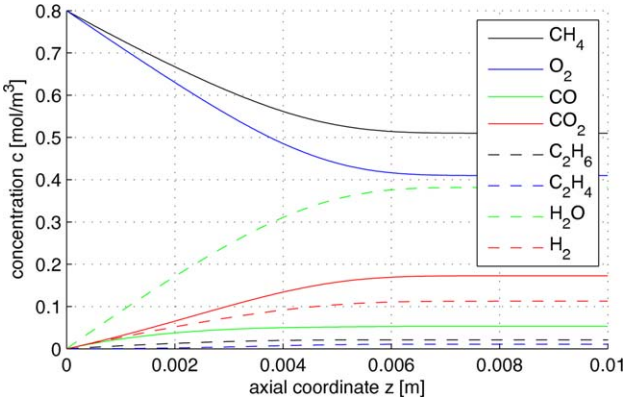

Figure 6. Concentration profiles for the FBR using a feed dilution of 87%.

[Color figure can be viewed in the online issue, which is available at wileyonlinelibrary.com.]

4. Another trend that has re-emerged is the increasing dilution of the shell-side gas flow with nitrogen. This can be understood as a further move toward near-isothermal reactor operation as the higher dilution eases the exothermic effects of the reactions.
5. Lastly, a steady decline in the diameter of both tube and shell is observed. Obviously, this again has two beneficial effects: First of all, the total heat caused by the reaction is smaller. On a smaller diameter the heat transfer through the reactor shell is more effective.

Overall, it appears that the C_2 hydrocarbon production depends mostly on an optimal temperature control and the presence of a small amount of oxygen in the packed-bed. Economically speaking, however, there is a trade-off between a higher yield through dilution, diameter reduction, and the actual amount of C_2 hydrocarbons obtained in a reactor. Smaller reactors and higher dilution would require more reactors in total and thus more effort when it comes to the actual product separation.

Finally, a few comments need to be made on some numerical issues:

1. After the intermediate step all further attempts to decrease the lower bounds on the temperatures have to be abandoned as the optimization just keeps running into either restoration phase failures or local infeasibilities.
2. The above noted optimization formulations and tasks required, in total, nearly three months to get to the last step.
3. For the last few tasks, the changes made to the variable bounds have to be chosen very carefully and the increases consequentially become ever smaller.

There are of course a number of inaccuracies in the implemented reactor model apart from the margins of error of all applied transport and fluid parameter correlations. One issue, in particular, has to be revisited: One reason for the excellent performance of the CPBMR might be a questionable applicability of the kinetics developed by Stansch et al.[14] Their kinetics have been formulated based on experimental data from the application of the OCM process in a microcatalytic FBR. As their reactor does not allow for continuous oxygen injection along the reactor length, the entire amount needs to be fed with methane. This obviously means that the oxygen concentrations at the inlet of the fixed-bed will always be higher than in a PBMR. Consequentially, Stansch et al. claim validity of their kinetics for oxygen partial pressures ranging from 1 to 20 kPa. This can lead to some minor trouble in a FBR whenever oxygen is consumed by the reaction mechanism and drops below 1 kPa, but it is almost certainly an issue from inlet to outlet in a PBMR. In the conventional feeding-mode, no oxygen is being injected to the tube-side of the membrane reactor. The only oxygen in the reactor tube-side arrives there by permeating the membrane from the shell-side. Accordingly, the oxygen partial pressure will always stay at quite low levels. In fact, it has been observed that whenever methane conversion is close to or larger than 50% in the CPBMR model, the oxygen level at every single collocation position is well below 1 kPa ranging from 0 to 500 Pa. As the parameters of the kinetics were not fitted for this range of partial pressures, it can easily be imagined that this leads to an overestimation (or possibly underestimation) of the reactor performance. Given how a PBMR works, there is however no way to guarantee oxygen levels of more then 1 kPa in the fixed bed–at least with this kinetic system. A closer look at the formation rates of all components for those low partial pressures of oxygen shows indeed a maximum for the formation of C_2 hydrocarbons for temperatures above 1000 K, well below 1000 Pa of oxygen. For details on this behavior see Figure 8. This, by no means, invalidates the kinetic system, but shows that a thorough experimental investigation is required.

Operation of the MRN

After the detailed analysis of the CPBMR's performance, this part focuses on the integration into the network and the joint performance thereof.

Implementation and performance of models

The FBR is expected to be considerably shorter than the CPBMR. Hence, only one heating/cooling segment is introduced. Methane and oxygen need to be fed to the reactor at the same inlet. Consequently, the concentration profiles can be expected to be steeper and temperature hot spots could be more of a problem as the higher oxygen concentration favors the oxidation reactions. This basically means that the length of individual finite elements needs to be a lot smaller and that more axial finite elements are required in comparison to the CPBMR.

Keeping the temperature in the reactor in check is a bit more of a challenge as feed dilution with nitrogen gas of more than 80% together with a catalyst dilution of one to four was necessary in previous work.[2, p.6350, fig. 17] For a feed dilution of 85%, methane conversion climbs to roughly 62.5%. However, selectivity is so low that there is close to no yield in C_2 products at all. For 87% dilution, this is fairly different: methane conversion is half as high at 33.8% and the yield in C_2 around 7.6%.

The higher oxygen levels in the tube-side of the PPBMR cause the same trouble as in the FBR, meaning that yet again a higher number of finite elements is required.

The required dilution with nitrogen found here is obviously quite high. This is, however, not necessarily unexpected. The best yield in C_2 hydrocarbons experimentally reported so far requires a dilution of methane with helium of 98% while allowing for a yield of 35% and a selectivity of 54% in a membrane reactor using a $Bi_{1.5}Y_{0.3}Sm_{0.2}O_{3-\Delta}$-catalyst.[30, p.908] Figures 6 and 7 show the concentration

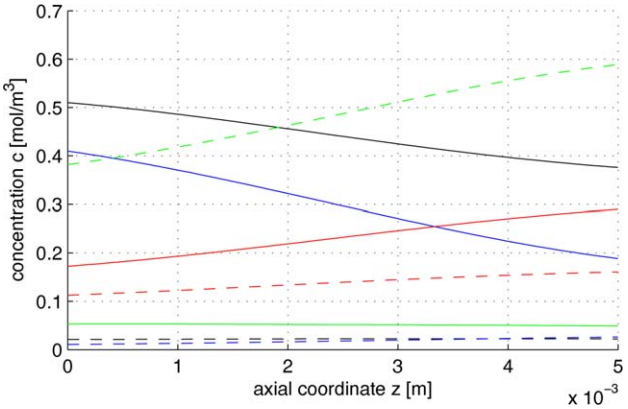

Figure 7. Concentration profiles for the PPBMR tube-side using a feed dilution of 87%.

For details on which line symbolizes which component, please refer to 6. [Color figure can be viewed in the online issue, which is available at wileyonlinelibrary.com.]

profiles for the reaction zones of both reactors at a feed dilution of 87%.

Network integration

For practical reasons, the network has basically only two different feed streams: the first containing methane, the second oxygen. Both gases will be diluted with nitrogen. This means that streams 2, 11, and 14 (see Figure 1) consist of the same molar fractions of oxygen and nitrogen, streams 1, 9, and 6 of the same molar fractions of methane and nitrogen.

As a starting point and to get a good match with the previously done simulations of FBR and PPBMR, each stream is diluted to a molar fraction of nitrogen of 87%. Because of recycle stream number 7 from the PPBMR shell-side to the CPBMR, tube-side superficial velocities in both FBR and PPBMR are reduced to 0.4 m/s to ensure that the same can stay below or at 1 m/s in the CPBMR.

The heating/cooling temperature in the CPBMR is slightly decreased to 950 K to prevent possible problems as a consequence of recycle stream number 7. Similarly, as a further precaution, the shell-side inlet temperature of the PPBMR is decreased to 900 K. Both stream 14, which is initially set to zero, and recycle stream 12, which will be activated to just 5% of its possible flow, can increase the oxygen concentration in the tube-side of the PPBMR, and thus, strengthen exothermic reactions. Table 3 contains the results of the network simulation for the configuration described earlier.

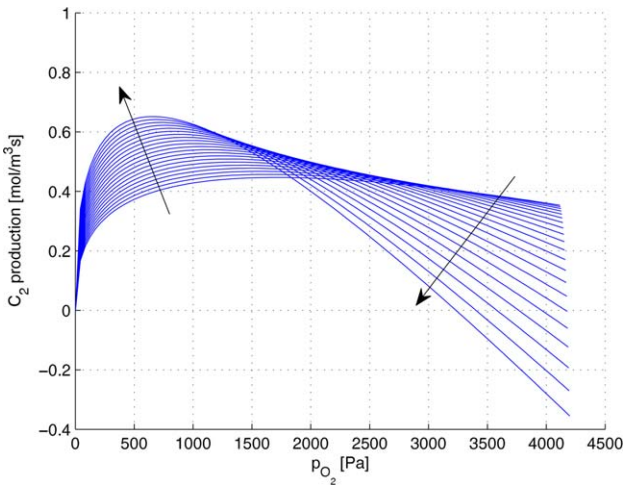

Figure 8. Rate of formation of C_2 products for various partial pressures of oxygen and different temperature levels.

[Color figure can be viewed in the online issue, which is available at wileyonlinelibrary.com.]

This point is obviously far from being an optimal solution as both methane conversion and yield in C_2 hydrocarbons of the network are lower than those for the individual CPBMR. Nevertheless, it is a good starting point in order to show that the network model actually works. The CPBMR in the network is probably close to the optimal solution found in the stand-alone optimization, because of the high dilution with nitrogen required by the other two reactors. The reduction of the superficial velocity in the FBR causes the temperature in that particular reactor to drop very quickly, thus, reducing the reaction rates to nearly zero after the first 2 mm of reactor length. The situation in the PPBMR is quite similar, although the reaction rates do not become completely zero before the reactor end.

General optimization

For the general optimization of the network, all geometrical and operational parameters mentioned for the CPBMR can be manipulated. In addition, more or less the same parameters are relevant for the other two reactors. The network itself offers some additional decision variables through the manipulation of recycle streams and the two feed streams. Initial sensitivity analyses at the aforementioned starting point show the appearance of numerous (local) infeasibilities brought along by the additional two reactors. Generally speaking, only the improvements described for the CPBMR above led to any improvements in the yield of C_2 hydrocarbons for the entire network. The sensitivity analysis would imply removing the additional reactors. However, this could simply be because of the excellent performance of the CPBMR at the starting point.

Further reactor investigation

The investigation on the CPBMR shows the necessity of its corresponding 2-D model. Given the size and complexity of the model for the network, only 1-D models are first used for the additional reactors. In order to further examine the implications of this simplification, 2-D models for both FBR and PPBMR are implemented.

Even after a few millimetres of reactor length, the results of 1-D and 2-D models deviate by several percentage points. The simultaneous feeding of oxygen and methane to the catalytic packed-bed leads to the formation of a hot-spot in the reactor center, which cannot be seen in the 1-D case.

In the case of the FBR, it might be possible to tune the behavior of the 1-D system to the 2-D, provided that the

Table 3. Results of the MRN Simulation

Component	Yield in C_2 Products	Selectivity in C_2 Products	Conversion of Methane
FBR	0.048	0.195	0.245
PPBMR	0.009	0.142	0.060
CPBMR	0.418	0.604	0.693
MRN	0.294	0.431	0.683

temperature can be controlled more effectively. The latter is not possible for the PPBMR. The diffusive flux through the membrane, yet again, necessitates the second dimension. A 2-D model for the entire network amounts to more than half a million variables and is currently under investigation.

Conclusions and Outlook

Simulations carried out as part of this work show that using a 2-D instead of just a 1-D model for the CPBMR is necessary and makes quite a difference at higher methane conversion rates. The advantages of the CPBMR in contrast to the FBR have become fairly obvious here. As was proven in the selectivity target investigation, it is possible to ensure both high yields of more than 40% and selectivities of more than 70% at the same time. The small influx of oxygen through the membrane prevents side reactions and helps keep the temperature increase in check at the same time. In addition, the influence of a heating/cooling system on the CPBMR has been tested. The configuration implemented here in combination with the feed dilution allows for almost isothermal temperature profiles in the reactor. These very helpful operating conditions can, however, not be implemented in FBR and PPBMR. The higher oxygen concentrations in the catalytic bed lead to barely controllable temperature spikes causing the oxygen to react fairly quickly and causing low yields in C_2 hydrocarbons. Further studies show that the radial temperature dependence cannot *a priori* be neglected in the FBR and is almost certainly an issue in the PPBMR because of the insulating effect of the shell-side.

In addition, a stable discretization method has been developed, which allows for the simultaneous optimization of highly nonlinear PDEs with both first- and second-order derivatives, without having to resort to a recurring simulation step. A sequential simulation method was developed to easily initialize complex collocated systems, without having to set up additional simulations using alternative discretization methods better suited for simulations.

Lastly, the influence of the range of validity of the kinetics on the obtained results was investigated, pointing to a necessity for a more careful derivation of the same and extending their applicability to very low partial pressures of oxygen.

Future work should focus on a number of issues: it needs to be investigated how important the influence of pressure loss, velocity fields, and axial dispersion on the reactor performance is. If indeed the models need to be extended even more, advanced model reduction techniques should be considered for future optimization approaches.

Efforts to extend kinetics to lower partial pressures of oxygen are under way in cooperation with the group of Prof. Schomäcker at TU Berlin.

Notation

c = concentration, mol/m^3
c_p = specific heat capacity, kJ/kg K
$\dot{c}r$ = component rate, mol/m^3 s
$\dot{h}$ = enthalpy flux, W/m^2,area specific enthalpy flow
k = heat transfer coefficient, W/m^2 K
ℓ = Lagrangian polynomial, –
$\dot{q}$ = heat flux, W/m^2, area specific heat flow
r = radius, radial coordinate, m
$\dot{r}r$ = reaction rate, mol/m^3 s, mol/g s, conversion rate of reactions, differs between gas phase and surface reactions
t = time, s
u_z = superficial velocity, m/s
z = axis, axial coordinate, m
$\mathcal{D}$ = diffusion coefficient, m^2/s
$\mathcal{H}$ = Hermite polynomial, –
$\dot{N}$ = molar flow, mol/s
T = temperature, K
ϕ = volume fraction, –
λ = thermal conductivity, W/m K
ϱ = density, kg/m^3
i, j, k = index variables, walk through components or reactions
$_r$ = radially
$_{cat}$ = catalyst
$_{cool}$ = variable belongs to heating/cooling system
$_{diff}$ = diffusion
$_{mix}$ = mixture
$_{shell,\ S}$ = shell-side
$_{tot}$ = total, e.g. sum or average over all species
$_{trans}$ = transfer, e.g. heat transfer through a membrane
$_{tube,\ T}$ = tube-side
$_G$ = gas
$_{OS}$ = outer shell
CPBMR = coventional packed-bed membrane reactor, packed-bed membrane reactor with a conventional feeding policy
FBR = fixed-bed reactor
MRN = membrane reactor network, network consisting of FBR, CPBMR, and PPBMR
PBMR = packed-bed membrane reactor
PPBMR = proposed packed-bed membrane reactor, membrane reactor with an alternative feeding policy

Literature Cited

1. Unruh D, Pabst K, Schaub G. Fischer-Tropsch synfuels from biomass: Maximizing carbon efficiency and hydrocarbon yields. *Energy Fuels*. 2010;24:2634–2641.
2. Jašo S, Godini H, Arellano-Garcia H, Omidkhah M, Wozny G. Analysis of attainable reactor performance for the oxidative methane coupling process. *Chem Eng Sci*. 2010;65:6341–6352.
3. Lafarga D, Santamaría J, Menéndez M. Methan oxidative coupling using porous ceramic membrane reactors – I. *Reactor Development. Chem Eng Sci*. 1994;49:2005–2013.
4. Quddus MR, Zhang Y, Ray AK. Multiobjective optimization of a porous ceramic membrane reactor for oxidative coupling of methane. *Ind Eng Chem Res*. 2010;49:6469–6481.
5. Chan PYP. Design and verification of catalytic membrane reactor for H_2 recovery from H_2S. Ph.D. thesis, The University of New South West Wales–The School of Chemical Science and Engineering, Sydney: Australia, 2007.
6. Godini H, Arellano-Garcia H, Omidkhah M, Karimzadeh R, Wozny G. Model-Based Analysis of reactor feeding policies for methane oxidative coupling. *Ind Eng Chem Res*. 2010;49:3544–3552.
7. Téllez C, Menéndez M, Santamaría J. Simulation of an inert membrane reactor for the oxidative dehydrogenation of butane. *Chem Eng Sci*. 1999;54:2917–2925.
8. Diakov V, Varma A. Optimal feed distribution in a packed-bed membrane reactor: The case of methanol oxidative dehydrogenation. *Ind Eng Chem Res*. 2004;43 (2):309–314.
9. Barbieri G, Maio FPD. Simulation of the methane steam re-forming process in a catalytic Pd-membrane reactor. *Ind Eng Chem Res*. 1997;36:2121–2127.
10. Chan PPY, Vanidjee K, Adesina AA, Rogers PL. Modeling and simulation of non-isothermal catalytic packed bed membrane reactor for H2S decomposition. *Catal Today*. 2000;63:379–385.
11. Al-Juaied M, Lafarga D, Varma A. Ethylene epoxidation in a catalytic packed-bed membrane reactor: experiments and model. 16th International Conference on Chemical Reactor Engineering. 2001; Issue 2:395–402.
12. Jašo S, Godini H, Arellano-Garcia H, Wozny G. Oxidative coupling of methane: reactor performance and operating conditions. In: Perucci S, editor. 20th European Symposium on Computer Aided Process Engineering–ESCAPE 20, Ferraris GB. 2010.
13. Tóta Á, Hlushkou D, Tsotsas E, Seidel-Morgenstern A. Packed-bed Membrane Reactors. In: Keil FJ, editor. Modeling of Process Intensification, chap. 5, WILEY-VCH Verlag GmbH Co. KGaA. 2007: pp. 99–148.
14. Stansch Z, Mleczko L, Baerns M. Comprehensive kinetics of oxidative coupling of methane over the La_2O_3/CaO catalyst. *Ind Eng Chem Res*. 1997;36:2568–2579.

15. Kleiber M, Joh R, eds. VDI-Wärmeatlas, 10th ed. Springer-Verlag, Berlin Heidelberg: 2006.
16. Fuller EN, Schettler PD, Giddins JC. A new method for prediction of binary gas-phase diffusion coefficients. *Ind Eng Chem.* 1966; 58(5):18–27.
17. Kee RJ, Coltrin ME, Glarborg P. Chemically Reacting Flow. Hoboken: Wiley-Interscience. 2003.
18. Tsotsas E, Schlünder EU. On axial dispersion in packed beds with fluid flow. *Chem Eng Process*. 1988;24(1):15–31.
19. Poling BE, Prausnitz JM, O'Connell JP. The Properties of Gases and Liquids. New York: McGraw-Hill. 2001.
20. Bauer R, Schlünder EU. Effective radial thermal conductivity of packing in gas flow. Part I. Convective transport coefficient. *Int Chem Eng*. 1978;18(2):181–188.
21. Bauer R, Schlünder EU. Effective radial thermal conductivity of packing in gas flow. Part II. Thermal conductivity of the packing fraction without gas flow. *Int Chem Eng*. 1978;18(2):189–204.
22. Specchia V, Baldi G, Sicardi S. Heat transfer in packed bed reactors with one phase flow. *Chem Eng Commun*. 1980;4:361–380.
23. Dixon AG. Wall and particle-shape effects on heat transfer in packed beds. *Chem Eng Commun*. 1988;71:217–237.
24. Biegler LT. Nonlinear Programming – Concepts, Algorithms, and Applications to Chemical Processes. Philadelphia, Pennsylvania: SIAM Society for Industrial and Applied Mathematics & MOS Mathematical Optimization Society. 2010.
25. Finlayson BA. Nonlinear Analysis in Chemical Engineering. New York: McGraw-Hill International Book Company. 1980.
26. Fourer R, Gay DM, Kernighan BW. AMPL – A Modeling Language for Mathematical Programming, 2nd ed. Broks/Cole: Thomson Learning, 2003.
27. Wächter A, Biegler L. On the implementation of an interior-point filter line-search algorithm for large-scale nonlinear programming. Math Program. 2005;Ser. A.
28. Hogg J. HSL Mathematical Software Library. Available at: http://www.hsl.rl.ac.uk/. 2011. Accessed 9-30-13.
29. Karypis G, Kumar V. METIS – Graph Partioning, Mesh Partioning, Matrix Reordering. Available At: Http://People.Sc.Fsu.Edu/~Jburkardt/C_Src/Metis/Metis.Html. 2006. Accessed 9-30-13.
30. Caro J. Membranreaktoren für die katalytische Oxidation. *Chemie Ingenieur Technik*. 2006;78(7):899–912.

Manuscript received Apr. 1, 2013, and revision received Sep. 20, 2013.